AMERICAN JOURNAL OF PHYSIOLOGY
HEART AND CIRCULATORY PHYSIOLOGY

*Am J Physiol Heart Circ Physiol* 324: H417–H429, 2023.
*First published January 27, 2023; doi:10.1152/ajpheart.00495.2022*

RESEARCH ARTICLE

*Considering Sex as a Biological Variable in Cardiovascular Research*

# Carotid dysfunction in senescent female mice is mediated by increased $\alpha_{1A}$-adrenoceptor activity and COX-derived vasoconstrictor prostanoids

**Tiago J. Costa,[1,4] Paula R. Barros,[1] Diego A. Duarte,[1,2] Júlio A. Silva-Neto,[1] Sara Cristina Hott,[1] Thamyris Santos-Silva,[1] Claudio M. Costa-Neto,[2] Felipe V. Gomes,[1] Eliana H. Akamine,[3] Cameron G. McCarthy,[4] Francesc Jimenez-Altayó,[5] Ana Paula Dantas,[6]* and Rita C. Tostes[1]***

[1]*Department of Pharmacology, Ribeirao Preto Medical School, University of São Paulo, Ribeirão Preto, São Paulo, Brazil;* [2]*Department of Biochemistry and Immunology, School of Medicine, University of São Paulo, Ribeirão Preto, São Paulo, Brazil;* [3]*Department of Pharmacology, Institute of Biomedical Sciences, University of São Paulo, São Paulo, São Paulo, Brazil;* [4]*Department of Cell Biology and Anatomy, Cardiovascular Translational Research Center, University of South Carolina, Columbia, South Carolina, United States;* [5]*Department of Pharmacology, Therapeutic, and Toxicology, School of Medicine, Neuroscience Institute, Universitat Autònoma de Barcelona, Bellaterra, Spain; and* [6]*Laboratory of Experimental Cardiology, Institut d'Investigacions Biomediques August Pi i Sunyer, Hospital Clinic Cardiovascular Institute, Barcelona, Spain*

## Abstract

α-Adrenergic receptors are crucial regulators of vascular hemodynamics and essential pharmacological targets for cardiovascular diseases. With aging, there is an increase in sympathetic activation, which could contribute to the progression of aging-associated cardiovascular dysfunction, including stroke. Nevertheless, there is little information directly associating adrenergic receptor dysfunction in the blood vessels of aged females. This study determined the role of a-adrenergic receptors in carotid dysfunction of senescent female mice (accelerated-senescence prone, SAMP8), compared with a nonsenescent (accelerated-senescence prone, SAMR1). Vasoconstriction to phenylephrine (Phe) was markedly increased in common carotid artery of SAMP8 [area under the curve (AUC), 527 ± 53] compared with SAMR1 (AUC, 334 ± 30, $P$ = 0.006). There were no changes in vascular responses to the vasoconstrictor agent U46619 or the vasodilators acetylcholine (ACh) and sodium nitroprusside (NPS). Hyperactivity to Phe in female SAMP8 was reduced by cyclooxygenase-1 and cyclooxygenase-2 inhibition and associated with augmented ratio of TXA2/PGI2 release (SAMR1, 1.1 ± 0.1 vs. SAMP8, 2.1 ± 0.3, $P$ = 0.007). However, no changes in cyclooxygenase expression were seen in SAMP8 carotids. Selective $\alpha_{1A}$-receptor antagonism markedly reduced maximal contraction, whereas $\alpha_{1D}$ antagonism induced a minor shift in Phe contraction in SAMP8 carotids. Ligand binding analysis revealed a threefold increase of α-adrenergic receptor density in smooth muscle cells (VSMCs) of SAMP8 vs. SAMR1. Phe rapidly increased intracellular calcium ($Ca_i^{2+}$) in VSMCs via the $\alpha_{1A}$-receptor, with a higher peak in VSMCs from SAMP8. In conclusion, senescence intensifies vasoconstriction mediated by $\alpha_{1A}$-adrenergic signaling in the carotid of female mice by mechanisms involving increased $Ca_i^{2+}$ and release of cyclooxygenase-derived prostanoids.

**NEW & NOTEWORTHY** The present study provides evidence that senescence induces hyperreactivity of $\alpha_1$-adrenoceptor-mediated contraction of the common carotid. Impairment of $\alpha_1$-adrenoceptor responses is linked to increased $Ca^{2+}$ influx and release of COX-derived vasoconstrictor prostanoids, contributing to carotid dysfunction in the murine model of female senescence (SAMP8). Increased reactivity of the common carotid artery during senescence may lead to morphological and functional changes in arteries of the cerebral microcirculation and contribute to cognitive decline in females. Because the elderly population is growing, elucidating the mechanisms of aging- and sex-associated vascular dysfunction is critical to better direct pharmacological and lifestyle interventions to prevent cardiovascular risk in both sexes.

*α-adrenergic receptor; cerebrovascular function; common carotid; menopause; senescence-accelerated mice*

## INTRODUCTION

Vascular dysfunction and the associated risk of cardiovascular diseases (CVD) increase with age in both men and women, although sex-associated differences exist regarding their incidence and severity of CVD. Cardiovascular diseases are less frequent in women at younger ages; however, they become more prevalent with aging (1). Since the elderly

*A. P. Dantas and R. C. Tostes jointly supervised this work.
Correspondence: A. P. Dantas (adantas@recerca.clinic.cat).
Submitted 7 September 2022 / Revised 18 January 2023 / Accepted 19 January 2023

population is growing worldwide, elucidating the mechanisms of aging- and sex-associated vascular dysfunction is critical for better direct pharmacological and lifestyle interventions to prevent cardiovascular risk in both sexes.

In the central nervous system, vascular aging induces functional and structural alterations of the brain circulation, contributing to the pathogenesis of cognitive impairment, Alzheimer's disease, eye disease (e.g., glaucoma), and stroke (2). Epidemiological studies have suggested that women have worse outcomes in neurovascular disease than age-matched men. Strokes are more severe and show higher case fatality at 1 mo among women (3). Moreover, women might have a higher burden of small vessel disease in the brain that could contribute to faster cognitive decline (4).

Classically, vascular dysfunction during aging is attributed to arterial stiffness or increased pulse wave velocity of large arteries (5), and endothelial dysfunction, in association with increased reactive oxygen species (ROS) generation and quenching of nitric oxide (NO) bioavailability (6). Moreover, an imbalance of COX-derived vasoconstrictor and vasodilator metabolites has also been implicated as an essential factor in the pathophysiology of vascular aging (7). In addition to endothelial dysfunction, increased resting sympathetic nerve activity has also been described with aging and pointed out as a crucial factor in the pathophysiology of hypertension and heart failure in the elderly (8, 9). Sympathetic fibers innervate peripheral and cerebral vasculature, and sympathetic discharge is a crucial regulator of vasomotor tone and homeostasis in several tissues, including the brain (10). Nonetheless, there is little information on how aging changes sympathetic signaling in the cerebrovascular circulation, and even less is known about how this effect would influence female cerebrovascular health. Therefore, further investigation into how aging affects the mechanisms of sympathetic vasoconstriction in females is warranted.

To address our knowledge about the influence of aging on adrenergic signaling in the cerebral vasculature, we used the senescence accelerated to study of vascular aging (11–13) and age-associated cognitive diseases (14, 15). This mouse model displays a spontaneous age-related deterioration of learning and memory compared with the control senescence-accelerated mouse resistant (SAMR1) strain (16). In the vascular system, ovariectomized SAMP8 females present vascular morphological alterations and endothelial dysfunction (11), and many of these abnormalities are not improved by estrogen treatment (17).

The brain vasculature consists of a dense network of arterioles that receive most of its supply from the carotid arteries system, which carry ~70% of the total cerebral blood flow (10). The cephalic circulation, mediated by the carotid artery, is an essential vascular bed to maintain adequate blood supply to the brain and prevent ischemia and tissue hypoxia. Therefore, the present study aims to determine the responses and mechanisms of $\alpha_1$-adrenergic subtypes activation in the carotid artery of females in nonsenescent (SAMR1) and senescent (SAMP8) mice. In this study, we hypothesized that isolated carotid arteries from senescent SAMP8 females present augmented specific $\alpha_1$-adrenergic responses compared with nonsenescent SAMR1.

## MATERIAL AND METHODS

### Animal Models

Female senescence-accelerated mouse-prone 8 (SAMP8, $n$ = 42) and senescence-accelerated mouse resistant (SAMR1, $n$ = 42) were obtained from the breeding stock of the Pharmacology Department at the Biomedical Sciences Institute of the University of Sao Paulo (ICB-USP), and the *Parc Scientific* of Barcelona. Mice were maintained according to institutional guidelines (constant room temperature of 22°C, 12-h:12-h light/dark cycles, 60% humidity, and standard mice chow and water ad libitum). All the procedures used in this study were approved and performed following the guidelines of the Ethics Committee of the Ribeirao Preto Medical School, University of Sao Paulo (number 267/2018) and the Ethics Committee of the University of Barcelona (Comitè Ètic d'Experimentació Animal, CEEA protocols: 134/12 and 583/14), following the *Guide for the Care and Use of Laboratory Animals*, published by the National Institutes of Health (NIH Publication, No. 85-23, Revised 1996). Mice were used at 6–9 mo of age and during the estrus phase of physiological estrous. The estrous cycle was determined by cell characterization in the vaginal smear. After euthanasia, carotid arteries were isolated for functional analysis, and abdominal fat, gastrocnemius muscle, and uterus were harvested for phenotypic analysis.

### Measurement of Sex Hormones

Blood was collected from the vena cava into heparin-containing tubes after isoflurane euthanasia (5%). Blood was centrifugated at 1,000 $g$ for 30 min at 4°C, and the supernatant was stored at −80°C until the experiments were performed. Plasma levels of estrogen (Cat. No. 10006315), progesterone (Cat. No. 582601), and testosterone (Cat. No. 582701) were determined by commercially available competitive ELISA assays (Cayman Europe) following the manufacturer's instructions.

### Determination of Arterial Blood Pressure

The indirect tail-cuff method was used to measure systolic blood pressure. After an initial adaptation process (preheated at 40°C for 5 min), systolic blood pressure was recorded and calculated as the average of three consecutive measurements.

### Novel Object Recognition Test

The novel object recognition (NOR) test determined cognitive function in SAMP8 (6 and 9 mo of age) and SAMR1 (9 mo) as described (18). Each animal was placed in the center of a circular arena (D60 cm × H60 cm) and allowed to explore it for 10 min for habituation. The next day, the NOR test was conducted in the same arena. Animals were subjected to two trials separated by 1 h. During the first trial (acquisition trial, T1), mice were placed in the arena containing two identical objects for 5 min. For the second trial (retention trial, T2), one of the objects presented in T1 was replaced by an unknown (novel) object. Animals were then placed back in the arena for 5 min. Object exploration was defined as the animal facing the object at ~2 cm distance while watching, licking, sniffing, or touching it

with the forepaws. Recognition memory was assessed using the discrimination index, corresponding to the difference between the time exploring the novel and the familiar object, corrected for the total time exploring both objects [discrimination index = (novel − familiar/novel + familiar)].

### Senescence Assay

Cellular senescence in mice vascular tissue was determined by β-galactosidase activity using a cellular senescence activity kit (Cell Biolabs, Cat. No. CBA231), according to the manufacturer's instructions. Briefly, pulverized aortic tissue from SAMR1 and SAMP8 was incubated with 100 μL of extraction buffer for 5 min under gentle shaking. Equal amounts of protein lysate (50 μg) were used to quantify the β-galactosidase staining. β-Galactosidase Assay Reagent was added to the samples for 30 min at 37°C. After this period, the reaction was stopped by adding 100 μL of β-galactosidase Assay Stop Solution to each sample. The fluorescence was read at 360 nm excitation and 465 nm emission using a plate reader immediately after incubation in a FlexStation fluorimeter coupled to the SoftMax Pro software (Molecular Devices, Sunnyvale, CA). Total protein was quantified by the Bradford method (Bio-Rad), and 18-mo-old C57Bl/6 mice lung was used as a positive control.

### Vascular Reactivity Studies

The common carotid arteries were dissected from anesthetized (Isoflurane, 4–5% induction; 1.5–2% maintenance) 8-mo-old SAMP8 and SAMR1 mice and cleaned from perivascular fat tissue and vagal innervation in ice-cold physiological salt solution (PSS) consisting of (in mM) 130 NaCl, 14.9 $NaHCO_3$, 4.7 KCl, 1.18 $KH_2PO_4$, 1.17 $MgSO_4$, 1.56 $CaCl_2{\cdot}2H_2O$, 0.026 EDTA, and 5.5 glucose. Carotid segments of 2 mm length with and without an intact endothelium were mounted in isometric wire myograph chambers filled with PSS warmed to 37°C and aerated with 95% $O_2$-5% $CO_2$. After a 30-min equilibration period and basal tension normalization, the common carotid segments were exposed three times (10-min intervals) to the receptor-independent depolarizing agent KCl (60 mM) until the contraction reached a stable plateau (~15 min) as previously described (17, 19). Endothelial integrity was tested by administration of a single concentration of acetylcholine ($10^{-6}$ M) after a contraction induced by phenylephrine (Phe, $10^{-6}$ M). Endothelium-intact arteries exhibited 60–80% of maximal relaxation, whereas endothelium-denuded arteries displayed less than 5% of relaxation. After washout and return to a stable baseline, arterial segments were exposed to increasing concentrations of phenylephrine ($10^{-9}$–$10^{-5}$ M, Sigma-Aldrich, P6126) and U46619 ($10^{-9}$–$10^{-5}$ M, Tocris, 1923), as well as the vasodilator agents acetylcholine (ACh, $10^{-9}$–$10^{-5}$ M, Sigma-Aldrich, A6625) and sodium nitroprusside (SNP, $10^{-9}$–$10^{-5}$ M). The contribution of the endothelium-derived factors to the vascular responses was determined by incubating carotid segments with one of the following inhibitors: *1*) nonselective nitric oxide synthase (NOS) inhibitor $N^{\omega}$-nitro-L-arginine methyl ester (L-NAME; $10^{-4}$ M), *2*) superoxide anion ($O_2^-$) scavenger (Tempol, $10^{-5}$ M), *3*) nonselective COX inhibitor (indomethacin, $10^{-6}$ M), *4*) selective COX-1 inhibitor (SC560, $10^{-5}$ M), or *5*) selective COX-2 inhibitor (NS398, $10^{-6}$ M). The contribution of specific α-adrenergic receptors to Phe-induced contraction was determined by treating arteries with an $\alpha_{1A}$-adrenergic antagonist (5-methyl-urapidil $10^{-8}$ – $10^{-6}$ M) and an $\alpha$-$_{1D}$ adrenergic antagonist (BMY 7378 $10^{-8}$–$10^{-6}$ M). Treatments with inhibitors and antagonists were done for 30 min before the Phe concentration-effect curve and the drugs were kept throughout the protocol.

Contractions to Phe and U46619 are shown as a percentage (%) of the contractile response induced by 60 mM KCl and relaxations to ACh, and SNP is expressed as the percentage (%) of contraction to U46619 ($10^{-7}$ M, ~50% $R_{max}$). The area under the concentration-response curve (AUC), maximal response ($E_{max}$), and half maximal effective concentration ($EC_{50}$) were used to measure cumulative responses induced by agonists in the presence of vehicle or specific drugs/inhibitors.

### Measurement of Prostaglandin Production by Aortic Rings

At the end of each protocol evaluating vascular reactivity to Phe, the Krebs medium was removed from the myograph chambers and left for 30 min at room temperature to allow the conversion of thromboxane $A_2$ ($TXA_2$) and prostacyclin ($PGI_2$) to their breakdown products: $TXB_2$ and 6-keto-PGF-1α, respectively. Samples were then frozen at −80°C. A commercial enzyme immunoassay kit determined levels of $TXB_2$, 6-keto-PGF-1α, and $PGF_2\alpha$ (Cayman Europe, $TXA_2$, Cat. No. 10004023; and $PGI_2$, Cat. No. 501100) following the manufacturer's instructions.

### α-Adrenergic Receptor Binding Assay

As previously described (19), binding experiments were performed in VSMCs from aortas of 8- to 10-mo-old SAMR1 and SAMP8. An equal number of cells (80,000) were seeded per well in six-well culture plates and incubated with cold binding buffer containing 25 mM Tris·HCl (pH 7.4) with 5 mM $MgCl_2$, 0.1% BSA, and 100 μg/mL bacitracin. Cells were incubated with 0.5 nM 7-methoxy-$^3$H-prazosin (PerkinElmer) for ~16 h at 4°C. Cells were then washed twice with cold wash buffer and lysed by adding lysis buffer (48% urea, 2% Nonidet P-40, 3 M acetic acid). Cell lysates were transferred to scintillation tubes, and after the addition of scintillation liquid (PerkinElmer) and vigorous mixing, the radioactivity was measured using the Tri-Carb 20100TR liquid scintillation counter (PerkinElmer). Nonspecific binding was obtained by radioactivity measurement in cells treated with 100 μM oxymetazoline. Total protein from lysates was quantified by the Bradford method (Bio-Rad). Specific binding was determined by total binding subtracted from nonspecific binding, which was calculated (GraphPad Software, San Diego, CA) to be expressed as fentmole of α-adrenergic receptor per milligram of protein.

### $Ca^{2+}$ Measurement in Vascular Smooth Muscle Cells

VSMCs were isolated from the aortas of 8-mo-old female SAMR1 and SAMP8. Cultures were maintained in Dulbecco's modified Eagle's medium (DMEM; Gibco-BRL) supplemented with 10% fetal bovine serum (FBS; Invitrogen). At the fourth passage, cells were plated in pretreated black-walled, clear-bottomed 96-well polystyrene plates (Corning,

NY) at a density of 40,000 cells/well in Dulbecco's modified Eagle's medium (DMEM) with 20% FBS and incubated for 24 h at 37°C in a 5% $CO_2$. Cytosolic-free calcium ($Ca^{2+}$) was measured using the cell-permeant Fluo-4 acetoxymethyl ester probe (Invitrogen, Cat. No. 14201). Following 24 h, the medium was replaced with ~430 μM Fluo-4 solution in DMEM and incubated in the dark for 45 min at 37°C. After washouts and a 15-min equilibration period, basal fluorescence was acquired at 494/506-nm excitation/emission using the FlexStation fluorimeter coupled to SoftMax Pro software (Molecular Devices, Sunnyvale, CA). After this period, the VSMCs were stimulated with phenylephrine $10^{-7}$ M, and the fluorescence was analyzed for 160 s. ionomycin calcium salt (Tocris, Cat. No. 1704) was used as a positive control. Inhibition of adrenergic receptor $\alpha_{1A}$ was performed in the presence of monoclonal rabbit IgG anti-$\alpha_{1A}$ antibody (Abcam, Cat. No. ab137123). A nonspecific IgG antibody was used as a negative control in this set of experiments.

### Quantitative Real-Time PCR

Changes in mRNA expression were quantified by Sybr green-based quantitative real-time (q)PCR, as previously described (20). The mouse-specific primer sequences were as follows: COX1 (NM_008969.3), forward: 5′-GAGCCGTGAGATGGGTGGGAGGG-3′, reverse: 5′-TGGATGTGCAATGCCAACGGCT-3′; and COX2 (NM_011198.3), forward: 5′-GTCAGGACTCTGCTCACGAAGGAAC-3′, reverse: 5′-ACAGCTCGGAAGAGCATCGCAG-3′. qPCR reactions were set following the manufacturer's conditions (Applied Biosystems-Thermo Fisher). Ct values obtained for each gene were normalized to Ct of housekeeping gene ACTB (ΔCt) and converted to the linear form using the term $2^{-\Delta Ct}$. Data were expressed as $2^{-\Delta\Delta Ct}$ relative to the average of SAMR1 expression.

### Statistical Analysis

Data are expressed as means ± SE. For analysis of vascular reactivity, individual concentration-effect curves were plotted on a sigmoidal curve by nonlinear regression analysis. The extra sum-of-squares $F$ determined the differences in the fit of concentration-response curves in all groups. The area under the curve (AUC) and $pD_2$ (negative logarithm of the $EC_{50}$ values—concentration that produces 50% of the maximum response) were calculated for individual contractile or relaxing concentration-response curves and expressed as arbitrary units. The contribution of different endothelium-derived factors to Phe-induced contractions was calculated by subtracting the AUC for Phe curves in the presence of inhibitors from the AUC for control Phe curves (Δ, change). Brown Forsythe and Welch ANOVA compared means across three (or more) independent variables, followed by Dunnett's T3 post hoc analysis for multiple comparisons. The comparison of means across SAMR1 versus SAMP8 and Basal versus treatments was performed by unpaired $t$ test with Welch's correction. In the cognitive test (NOR), all the data were subjected to tests to verify the homogeneity of variances (Bartlett's test) and if they followed a normal distribution (Shapiro–Wilk test). Those that met these parameters were subjected to parametric analysis (one-way ANOVA followed by Tukey's posttest). The statistical analysis was carried out using the Prism 9 software (GraphPad Software, San Diego, CA), and statistical significance was accepted at $P < 0.05$.

## RESULTS

### Basic Parameters Analyses

Senescent SAMP8 display a distinct metabolic profile, with increased abdominal obesity, decreased lean mass, and increased body weight in comparison to SAMR1 (Table 1, Supplemental Fig. S1; http://doi.org/10.6084/m9.figshare.21065662). The groups had similar levels of estrogen, testosterone, and progesterone (Table 1). Interestingly, despite showing similar hormone levels, the uterine weight was decreased in SAMP8 compared with SAMR1, and female SAMP8 spent less time in estrus than SAMR1 (Table 1, Supplemental Fig. S1). There were no differences in blood pressure levels between SAMR1 and SAMP8 (Table 1).

Cognitive function was determined by the NOR test (Supplemental Fig. S2*A*). During the habituation session, there were no differences in locomotor activity between the groups (Supplemental Fig. S2*B*). Although there was no difference between the exploration of the familiar objects placed on the right or left side of the arena during the training trial, SAMP8 (both at 6 and 9 mo of age) spent more time exploring the objects than SAMR1 (Supplemental Fig. S2*C*), indicating a lack of spatial preference. In the retention trial, a greater exploration of the novel object was observed in 9-mo-old (9 M) SAMR1 ($t_{22}$ = 4.260, $P < 0.0003$) and 6-mo-old (6 M) SAMP8 ($t_{22}$ = 4.830, $P < 0.0002$), but not in 9 M SAMP8 ($t_{22}$ = 1.264, $P > 0.05$; Supplemental Fig. S2*D*). These findings were reflected in the discrimination index (Supplemental Fig. S2*E*), showing a lower cognitive function in SAMP8 at 9 mo compared with younger SAMP8 (6 mo) and its respective nonsenescent control SAMR1 at 9 mo. In addition to cognition, the arteries of 8-mo-old SAMP8, early state of lower cognition, presented signs of senescence in arteries as determined by increased β-galactosidase activity compared with SAMR1 (Supplemental Fig. S3), and for the next sets of experiments, SAMP8 and SAMR1 were tested at 8 mo of age.

### Vascular Reactivity in the Carotid Artery

In carotid arteries of 8-mo-old female SAMP8, the contractile responses to Phe were markedly increased compared

**Table 1.** *Basic parameters of 8-mo-old SAMR1 and SAMP8 female mice*

| | SAMR1 | SAMP8 |
|---|---|---|
| Body weight, g | 25.8 ± 0.4 | 30.6 ± 0.7* |
| Abdominal fat, mg tissue/cm tibia | 0.19 ± 0.05 | 0.42 ± 0.03* |
| Gastrocnemius dry, mg tissue/cm tibia | 0.029 ± 0.002 | 0.0016 ± 0.002* |
| Uterus dry, mg tissue/cm tibia | 0.023 ± 0.003 | 0.010 ± 0.001* |
| Tail-cuff blood pressure, mmHg | 113 ± 3 | 107 ± 7 |
| Estrogen, pg/mL | 9.25 ± 2.5 | 7.04 ± 1.13 |
| Progesterone, pg/mL | 68.35 ± 45 | 72.97 ± 86 |
| Testosterone, ng/mL | 6.65 ± 13.3 | 6.85 ± 4.5 |

Values are means ± SE of 5 animals/group. Statistical significance was calculated by unpaired $t$ test with Welch's correction. *$P < 0.05$ vs. SAMR1.

with age-matched SAMR1, as demonstrated by the greater AUC and maximal contraction in vessels with (Fig. 1*A*, Supplemental Table S1) or without endothelium (Supplemental Fig. S4 and Supplemental Table S1). On the other hand, there were no differences in the contractile responses to U46619 (Fig. 1*C*) or in the vasodilation to ACh (Fig. 1*D*) and SNP (Fig. 1*E*) in the common carotid rings of the SAMR1 and SAMP8 groups.

Next, we sought to elucidate the mechanisms involved in the Phe hypersensitivity found in the common carotid artery of SAMP8. We analyzed the contribution of the main endothelium-derived factors to the contractile response to Phe. Nonselective inhibition of NO production with L-NAME increased the vasoconstrictor responses to Phe in carotids of both SAMR1 (Fig. 2*A*) and SAMP8 (Fig. 2*B*). In addition, scavenging of superoxide anion ($O_2^-$) with Tempol decreased Phe contractions in common carotids from SAMP8 (Fig. 2*D*) but did not affect the contractions in the carotid of SAMR1 (Fig. 2*C*). Carotid arteries were initially treated with the nonspecific inhibitor of cyclooxygenases (COX) indomethacin, to determine the contribution of COX-derived prostanoids to the regulation of Phe-induced contractions in SAMP8. Indomethacin decreased Phe contraction in carotid arteries of SAMP8 (Fig. 2*F*), but not in SAMR1 arteries (Fig. 2*E*). The relative contribution of each endothelium-derived factor (NO, $O_2^-$, or prostanoids) was analyzed by calculating the change in the AUC (Fig. 2*G*). This analysis showed an equal contribution of NO to the contractile responses to Phe in the arteries of SAMR1 and SAMP8. However, change in the AUC after COX inhibition was significantly increased in the SAMP8 group, suggesting a contribution of COX-derived vasoconstrictor metabolites to the vascular hyperreactivity to Phe in female SAMP8. No differences in the change in the AUC after Tempol treatment were observed between the groups (Fig. 2*G*).

The specific role of COX isoenzymes in Phe contractions was then determined by incubating SAMR1 and SAMP8 carotids with the selective inhibitors of COX-1 (SC560) and COX-2 (NS398). Following the indomethacin response pattern, selective COX-1 and COX-2 inhibition did not modify Phe-induced contractions in vessels of SAMR1 (Fig. 3, *A* and *B*). On the other hand, in SAMP8, the inhibition of COX-1 and

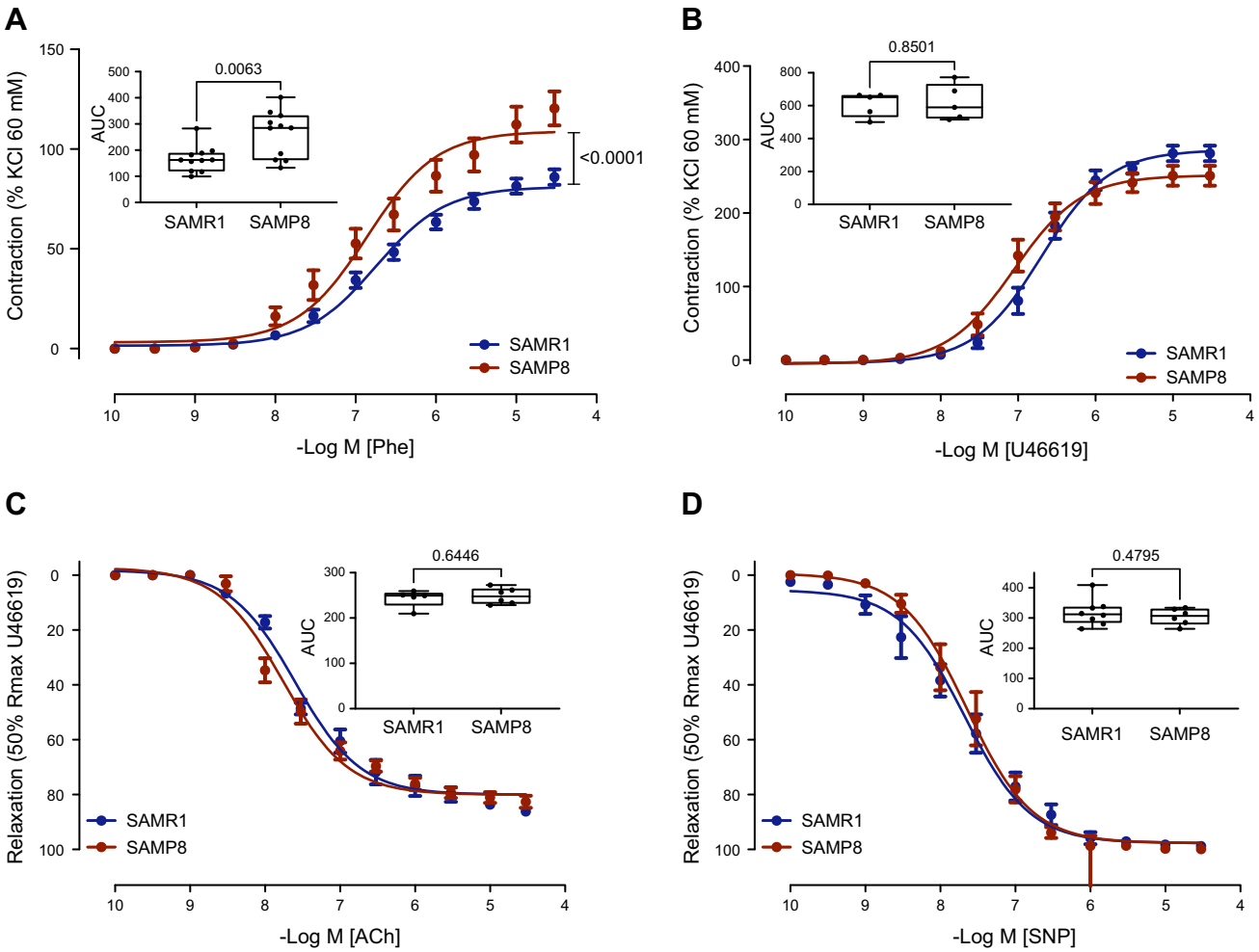


**Figure 1.** Senescence induced changes in adrenergic vasocontraction. Cumulative concentration-response curves to phenylephrine (Phe; *A*), U46619 (*B*), acetylcholine (ACh; *C*), and sodium nitroprusside (SNP; *D*) in endothelium-intact common carotid artery from 8-mo-old SAMR1 and SAMP8 females. *Insets*: graphs are means ± SE of the area under the curve calculated from each concentration-response curve ($n$ = 6–11 mice/group). Statistical significance was calculated by the extra sum-of-squares $F$ (fit of concentration-response curves) and $t$ test with Welch's correction (AUC). $P$ values and comparisons are expressed on top of box and whiskers plots and by the curves. Significance is considered when $P < 0.05$. AUC, area under the crurve.

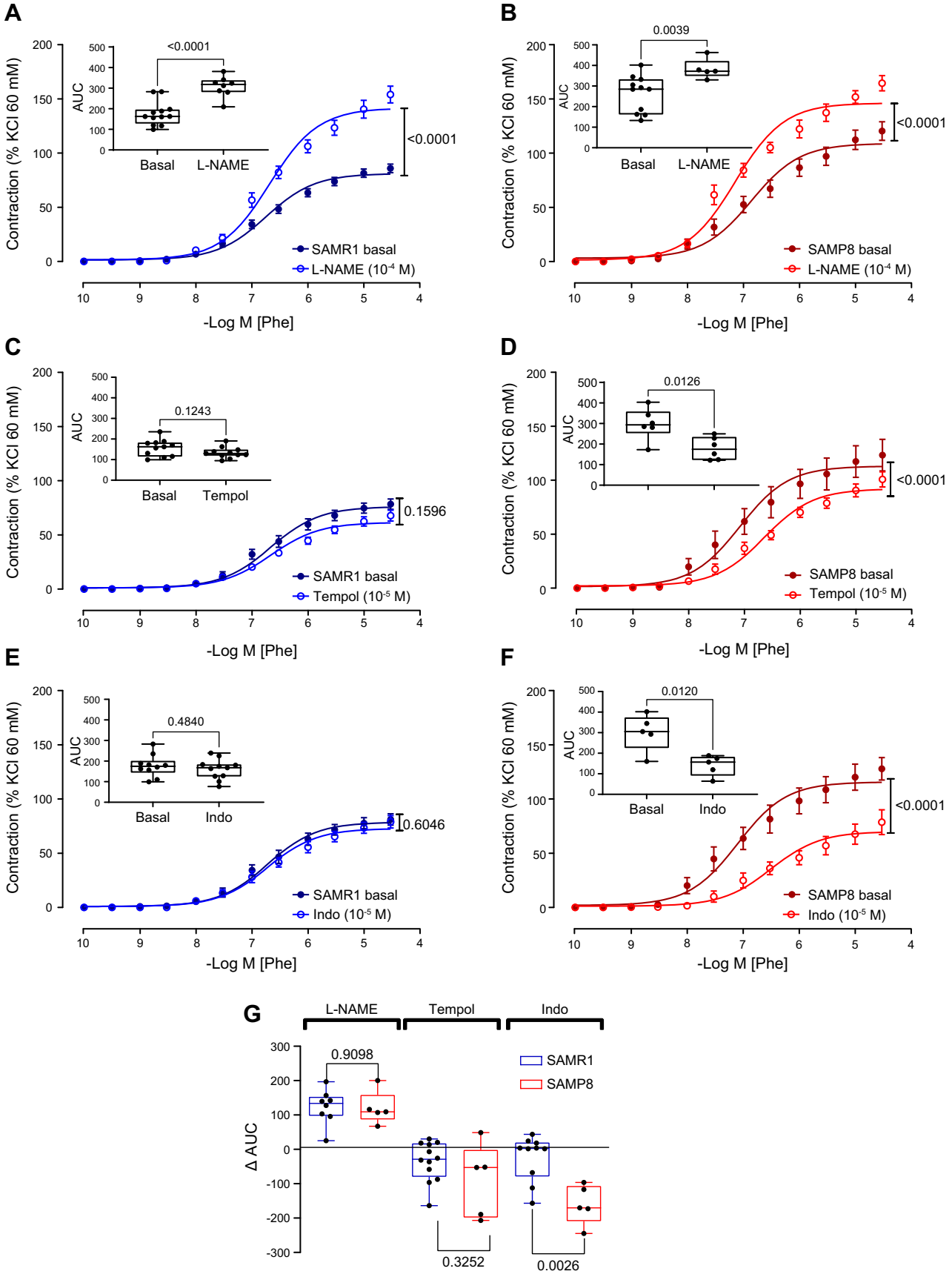

COX-2 decreased Phe-induced vasoconstriction (Fig. 3, *C* and *D*), suggesting increased production of COX-derived vasoconstrictor prostanoids in the carotid arteries of senescent mice. Prostanoid release from the common carotid artery was determined in the Krebs solution collected after concentration-response curves to Phe. In carotids from SAMP8, the release of $PGI_2$ was decreased by approximately twofold compared with SAMR1 arteries (Fig. 3*E*). Although the release of $TXA_2$ by Phe was similar between the groups (Fig. 3*F*), the $TXA_2/PGI_2$ ratio was two times higher in SAMP8 than in SAMR1 (Fig. 3*G*), which could favor the more pronounced vasoconstriction in SAMP8 carotid arteries. Despite the differences in COX pathway activation, there were no changes in the expression of COX-1 (Fig. 3*H*) or COX-2 (Fig. 3*I*) in the common carotid of SAMP8 versus SAMR1.

### Role of $a_1$-Adrenergic Receptor in the Vascular Hyperreactivity to Phe in SAMP8

In another set of experiments, carotids were treated with selective antagonists of $\alpha_{1A}$ (5-methyl-urapidl) and $\alpha_{1A}$ (BMY7378) receptors to determine the role of the α-adrenoceptors' subtypes in the vascular hyperreactivity to Phe in SAMP8. Different concentrations of both antagonists were tested in the common carotid of SAMR1 to establish the antagonist concentration used in the studies (Fig. 4, *A* and *B*). In arteries of SAMR1, the addition of $10^{-7}$ M of the $\alpha_{1A}$ (Fig. 4*C*) or $\alpha_{1A}$ (Fig. 4*D*) antagonists right-shifted the concentration-dependent curves to Phe, showing that both receptors contribute to Phe-induced contraction. However, in the carotid of SAMP8, $\alpha_{1A}$ antagonism blunted the maximal contraction to Phe (Fig. 4*E*), whereas $\alpha_{1A}$ antagonism induced a minor shift in Phe contraction (Fig. 4*F*). The density of $\alpha_1$-adrenergic receptor was analyzed in primary VSMC cultures of female SAMR1 and SAMP8. A single concentration of [$^3$H]-prazosin was used to generate association binding in the absence (total biding) or in the presence of 100 μM Oxymetazoline (for nonspecific biding; Fig. 4*G*). Following normalization of [$^3$H]-prazosin counts (cpm) with the amount of protein in each sample, we observed a marked increase in the affinity of $\alpha_1$-adrenoreceptor in VSMCs of SAMP8 (Fig. 4*H*), suggesting a higher density of the receptor.

Continuing the studies of $\alpha_1$-adrenoreceptor activity in VSMCs of SAMR1 and SAMP8, we determined changes in intracellular $Ca^{2+}$ ($Ca_i^{2+}$) following activation of $\alpha_1$ receptor with $10^{-7}$ M Phe (Fig. 5*A*). Although Phe induced a rapid increase of $Ca_i^{2+}$ in both groups, the peak of $Ca_i^{2+}$ was significantly higher in VSMCs from SAMP8 than in SAMR1 VSMCs (Fig. 5, *B*–*E*). Blockade of the $\alpha_{1A}$-receptor with a monoclonal antibody augmented Phe-induced $Ca_i^{2+}$ in VSMCs from SAMR1 (Fig. 5, *C* and *E*), whereas it decreased $Ca_i^{2+}$ in cells from SAMP8 (Fig. 5, *D* and *E*).

## DISCUSSION

This study shows that the conductance artery carotid from senescence females present higher levels of adrenergic receptors and hyperactivity in response to α-adrenergic receptor stimulation. At the beginning of senescence in the female SAMP8 model [as established in our previous studies (11)], there are increased constrictor responses to Phe in the carotid arteries mediated by $\alpha_{1A}$-adrenoceptor that in turn increase $Ca^{2+}$ influx. In addition, this study observed changes in prostanoid unbalance under Phe stimulus in the carotid of SAMP8 than SAMR1, which impact Phe-induced vasoconstriction. To the best of our knowledge, no study has described the specific α-adrenergic subtype mechanisms in the carotid arteries of senescent females at the functional and molecular levels. So far, only a few functional studies on aging-associated sympathetic hyperactivity have focused on the carotid vascular bed (21–23).

Senescence, per se, is known to cause a series of alterations in the endogenous mechanisms that control cellular function leading to a subsequent increase in organ dysfunction and the risk of cardiovascular disease. A correlation between senescence and vascular dysfunction has been extensively described in men and women and has been primarily associated with decreased NO-mediated vasodilation (24) and platelets-derived NO (25). However, as reviewed by Barros et al. (26), the physiological mechanisms that control vascular function during senescence differ in males and females (26).

The female senescence-accelerated mouse prone is an experimental model that exhibits characteristics of senescence-associated dysfunction, including cognitive (14) and vascular alterations (12). In addition, reproductive senescence in this model is associated with ovarian decline characterized by periods of constant estrus cycle and lack of ovulation (27). Despite not exhibiting changes in sex hormone levels, female SAMP8 spend more time in diestrus than estrus (12) at younger ages (28) in comparison to SAMR1. In association with estrus cycle dysregulation, we observed a reduction in uterine weight, increased abdominal fat, and decreased gastrocnemius mass in SAMP8 compared with SAMR1 mice. These characteristics are similar to those seen in postmenopause women (29).

In this study, we found that vasoconstriction induced by the α-adrenergic agent Phe was the only response modified in the carotid arteries of SAMP8 at 8 mo. There were no differences in the contractile responses to U46619 or vasodilation to ACh or NPS in the carotids of SAMP8 compared with SAMR1. In previous studies, we observed changes in vascular reactivity to the vasoconstrictor agent U46619 and to the endothelium-dependent vasodilator ACh in the aorta of female SAMP8 (11–13), suggesting a different mechanism in carotid and aorta dysfunction.

**Figure 2.** Impact of senescence on endothelium-derived factors and phenylephrine (Phe) contraction. Cumulative concentration-response curves to Phe in endothelium-intact common carotid artery from 8-mo-old SAMR1 and SAMP8 females. The role of NO, $O_2^-$, and prostanoids in Phe-induced contraction was assessed by treatment with L-NAME (*A* and *B*), Tempol (*C* and *D*), and indomethacin (*E* and *F*). *Insets*: graphs are means ± SE of the area under the curve calculated from each concentration-response curve ($n$ = 6–12 mice/group). *G*: delta difference in the AUC of basal vs. treated arteries. Statistical significance was calculated by the extra sum-of-squares $F$ (fit of concentration-response curves) and $t$ test with Welch's correction (AUC). $P$ values and comparisons are expressed on top of box and whiskers plots and by the curves. Significance is considered when $P < 0.05$. AUC, area under the crurve.

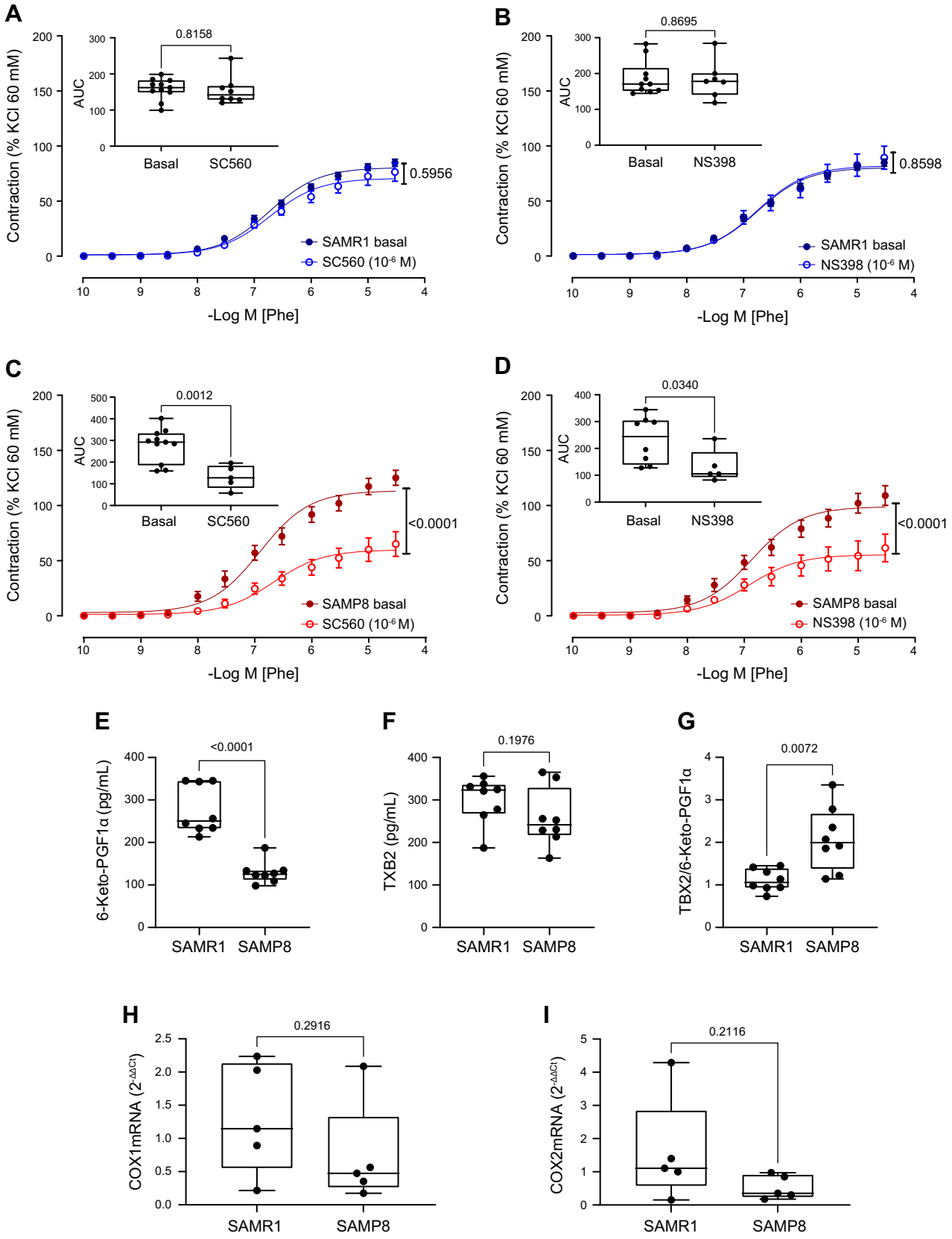



*AJP-Heart Circ Physiol* • doi:10.1152/ajpheart.00495.2022 • www.ajpheart.org

Differences in functional responses among the vascular beds may be related to their diverse origin and structures. In preliminary studies in female SAMP8, changes in vascular reactivity were determined in the descending thoracic aorta (developed from the somites). In contrast, in the present study, vasoactive responses were determined in the common carotid arteries that are branches of the brachiocephalic artery deriving from ascending aortic arch [with the origin in the neural crest (30)]. A detailed study on the structural, genetic, and functional heterogeneity of VSMCs of a unique aorta demonstrated that cells from different embryonic origins are functionally distinct (31). Therefore, the existence of a fingerprint of vascular function and dysfunction in each vascular bed is recognized, which must depend on the origin and environment in which the vessel is surrounded.

Different intrinsic mechanisms have been described to contribute to altered vascular responses in senescent vessels. The aorta of female SAMP8 presented an earlier, faster, and time-dependent decrease in NO and increased oxidants levels compared with SAMR1 (11–13), which may contribute to the observed aortic dysfunction. Yet, unlike other models of senescence or vascular beds in the same model, COX-derived metabolites were the only endothelium-derived factors modified in SAMP8 carotid arteries. Changes in Phe-induced contractions in female SAMP8 were associated with an increased ratio of the release of vasoconstrictors over vasodilator prostanoids. The higher $TXA_2$-to-$PGI_2$ ratio after Phe stimulation in the carotids of SAMP8 may favor the greater vasoconstriction observed. However, granting that the imbalance in prostanoid biosynthesis justifies the existence of vascular dysfunction in carotid arteries of SAMP8, this result does not explain why this dysfunction is unique to Phe responses, as there is no difference in the responses to other vasoactive agents, such as the vasoconstrictor U46619, a $TXA_2$ analog, or the endothelium-dependent vasodilator ACh. A possible contribution of alternative pathways, such as the EDHF, could also provide a transitory compensatory response in the common carotid at this age range. This hypothesis has not, however, been tested by us or other groups to date.

Chronic overactivity of the sympathetic nervous system is a hallmark of aging and contributes to the development of several aging-associated diseases, including cardiovascular diseases (8). Over the last few decades, the neuronal mechanisms contributing to sympathetic overactivity were studied in detail only with limited success under pathophysiological conditions. Moreover, most studies present a more neurological than vascular approach (8).

The α-adrenergic signaling pathway is one of the central regulators of cerebrovascular tone and cerebral blood flow, and α-adrenergic vascular responses change with age, although not equally in the different vascular territories within the brain vasculature (32). In our study, we showed that vascular dysfunction of carotid arteries at early stages of senescence in female SAMP8 is associated with hyperactivity in response to adrenergic signaling in the vascular smooth muscle, rather than only endothelial dysfunction (12). Increased Phe-induced contraction was observed in endothelium-intact and endothelium-denuded carotid arteries. We also observed a marked increase in binding affinity to $\alpha_1$-adrenoreceptor that was paralleled by $\alpha_{1A}$-mediated increased $Ca^{2+}$ influx in vascular smooth muscle cells isolated from SAMP8. Our results and a few other studies in this field show that sympathetic regulation of cerebral circulation during aging is not a direct and uniform process and may vary depending on the vascular bed and pathophysiological conditions.

With aging, cognitive impairment results from nonvascular processes and vascular dysfunction (33). In the present study, we observed that the onset of carotid vascular dysfunction is associated with impairments in cognitive function, reflected by the lower discrimination index observed in senescent females (9-mo-old SAMP8) in the NOR test. Most studies on the vascular mechanisms of cognitive impairment are related to small vessel diseases that manifest as dysregulated neurovascular coupling and blood-brain barrier dysfunction (33, 34). Nonetheless, we cannot minimize the role of conductance arteries in microvascular dysfunction. Studies have suggested that carotid artery dysfunction, such as stenosis, is an independent risk factor for cognitive impairment and cardiovascular disease (35–39).

Although the carotid arteries do not have direct contact with the brain, they are essential suppliers of blood to the brain via the circle of Willis and key controllers of cerebral blood flow (36). Moreover, it is well established that changes in vascular contractility and elasticity of conductance vessels (including carotid arteries) modify the pattern of flow and pulsatility toward smaller vessels, modifying their vascular tone. In a prospective and community-based study, Mitchell et al. (40) described that reduced wave reflection at the interface between the carotid and aorta leads to the transmission of excessive flow pulsatility into the brain, microvascular structural brain damage, and lower scores in various cognitive domains. In addition, this study showed that changes in carotid pulse pressure were associated with lower memory scores in this population. In the present study, despite the parallelism of the α-adrenergic hyperactivity in the common carotid with cognitive decline in senescent female mice, we are aware that our results do not directly test the contribution of changes in carotid adrenergic reactivity to cognition decline. Nonetheless, this study provides new insights into potential mechanisms for vascular-associated cognitive impairment during aging.

**Figure 3.** Impact of senescence on COX-mediated signaling pathway. Cumulative concentration-response curves to phenylephrine (Phe) in endothelium-intact common carotid artery from 8-mo-old SAMR1 and SAMP8 females. The role of COX-1- and COX-2-derived prostanoids to Phe-induced contraction was assessed by treatment with selective COX-1 (*A* and *C*) or COX-2 (*B* and *D*) inhibitors. *Insets*: graphs are means ± SE of the area under the curve calculated from each concentration-response curve ($n$ = 6–11 mice/group). The levels of prostacyclin (*E*), thromboxane $A_2$ (*F*), and the ratio of release (*G*) were determined after concentration-response curves to Phe. The expression of mRNA of COX-1 (*H*) and COX-2 (*I*) was determined in the common carotid of SAMR1 and SAMP8. Statistical significance was calculated by the extra sum-of-squares $F$ (fit of concentration-response curves) and $t$ test with Welch's correction (AUC). $P$ values and comparisons are expressed on top of box and whiskers plots and by the curves. Significance is considered when $P < 0.05$. AUC, area under the crurve.

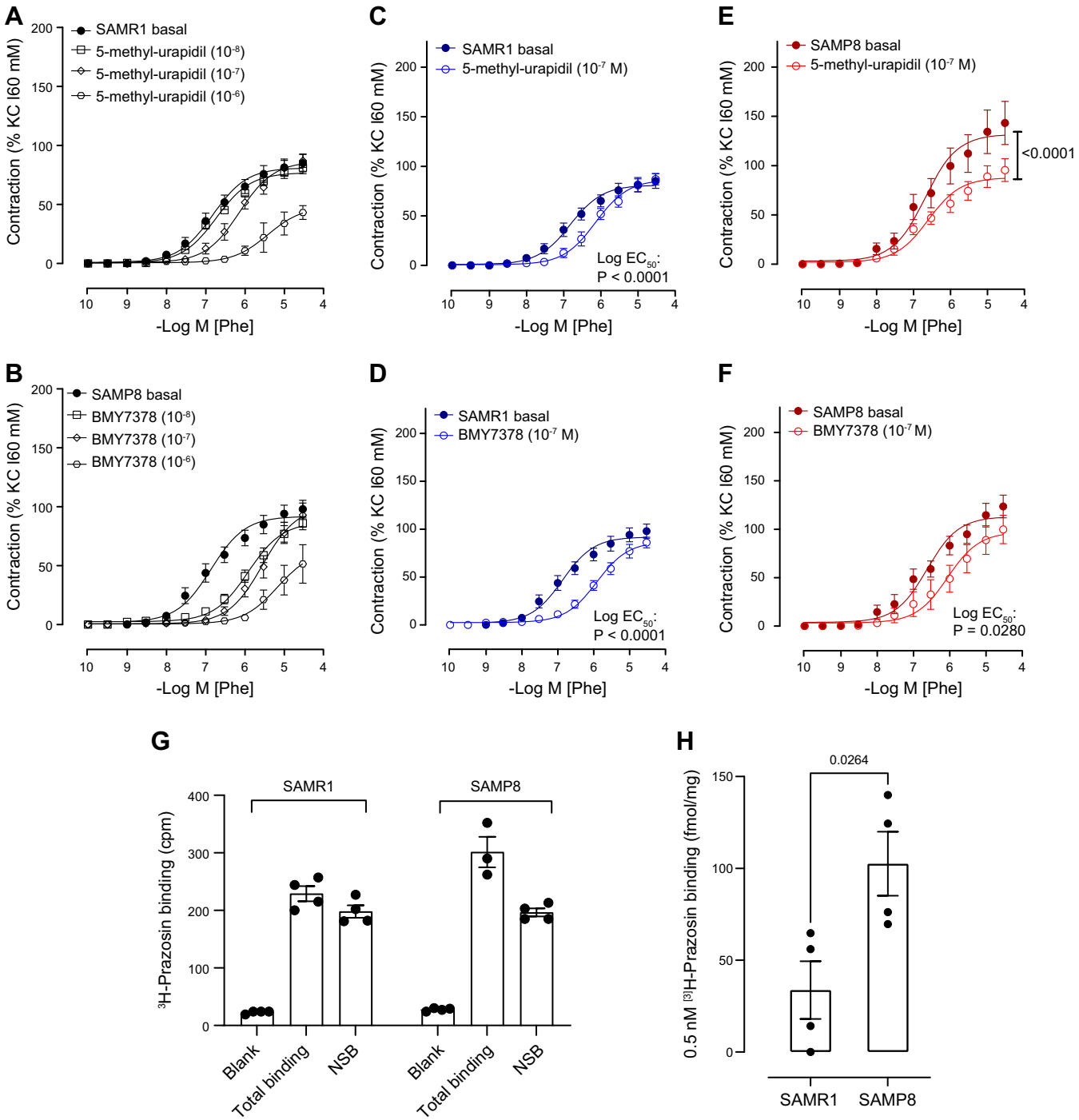


**Figure 4.** Role of senescence on $a_1$-adrenergic receptor-mediated contraction. Cumulative concentration-response curves to phenylephrine (Phe) in endothelium-intact common carotid artery from 8-mo-old SAMR1 and SAMP8 females. The contribution of specific α-adrenergic receptors to Phe-induced contraction was determined by pretreatment of arteries with $\alpha_{1A}$-adrenergic antagonist (5-methyl-urapidil, $n$ = 8) and $\alpha_{1D}$-adrenergic antagonist (BMY 7378, $n$ = 8). The antagonist concentrations of 5-methyl-urapidil (*A*) and BMY 7378 (*B*) to be used in the studies concertation were tested in the common carotid of SAMR1 and then tested as a single concentration ($10^{-7}$ M) in the common carotid of SAMR1 (*C* and *D*) and SAMP8 (*E* and *F*). The density of $\alpha_1$-adrenergic receptors was determined in the primary culture of VSMCs from SAMR1 and SAMP8 (*G*) and normalized by the amount of protein (*H*). Statistical significance was calculated by the extra sum-of-squares *F* (fit of concentration-response curves) and *t* test with Welch's correction (receptor density and $EC_{50}$). *P* values and comparisons are expressed on top of box and whiskers plots and by the curves. Significance is considered when $P < 0.05$. VSMCs, smooth muscle cells.

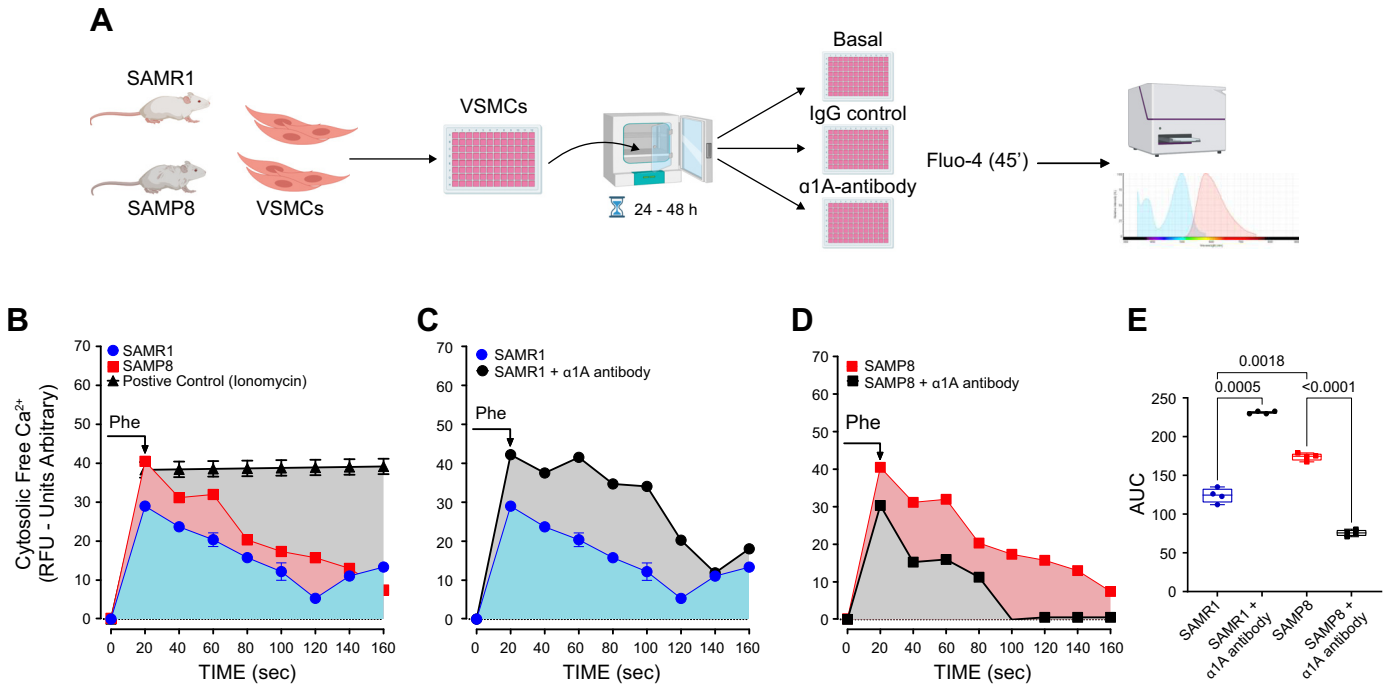


**Figure 5.** Senescence increases intracellular free calcium via the $\alpha_{1A}$-adrenergic receptor. *A*: schematic representation of protocol for determining intracellular free calcium ($Ca_i^{2+}$) in response to Phe ($10^{-7}$ M) in VSMCs of SAMR1 and SAMP8 female mice. *B*: time-course of $Ca_i^{2+}$ in response to Phe stimuli ($10^{-7}$ M) in VSMCs of SAMR1 and SAMP8, and in response to ionomycin, as a positive control. *C* and *D*: time course of $Ca_i^{2+}$ in the absence and the presence of $\alpha_{1A}$ antibody in VSMCs of SMAR1 (*C*) and SAMP8 (*D*). *E*: box and whiskers plots show the differences in the AUC of $Ca_i^{2+}$ time course in all groups ($n$ = 4 individual sample/group). Statistical significance was calculated by Brown Forsythe and Welch ANOVA, followed by Dunnett's T3 post hoc analysis. *P* values and comparisons are expressed on top of box and whiskers plots. Significance is considered when $P < 0.05$. *A* was created using a licensed version of BioRender. AUC, area under the crurve; VSMCs, smooth muscle cells.

### Conclusions

The present study provides evidence of increased $\alpha_{1A}$-adrenoceptor signaling, linked to a functional impairment of common carotid of the female murine model of senescence (SAMP8). Increased α-adrenergic reactivity of the common carotid artery during senescence is paralleled with cognitive decline in senescent females and may represent a potential mechanism for cognitive dysfunction with aging. Although our results do not provide direct evidence to associate carotid dysfunction with cognitive impairment, it furnishes the rationale for the design of further experiments to determine the mechanisms of vascular senescence in cerebral dysfunction.

## DATA AVAILABILITY

Data will be made available upon reasonable request.

## SUPPLEMENTAL DATA

Supplemental Figs. S1–S3 and Supplemental Table S1: http://doi.org/10.6084/m9.figshare.21065662.

## ACKNOWLEDGMENTS

We thank Carla P. Manzato for excellent technical assistance and Dr. Andre Sampaio Pulpo for excellent discussion and suggestions in the analysis of α-adrenergic receptors and the binding technique. Graphical abstract was created using a licensed version of BioRender.

## GRANTS

This study was supported by Fundação de Amparo à Pesquisa do Estado de São Paulo (FAPESP) Grant 2013/08216-2 (to R.C.T.) to the Center of Research in Inflammatory Disease; Conselho Nacional de Desenvolvimento Científico e Tecnológico (CNPq); Coordenação de Aperfeiçoamento de Pessoal de Nível Superior (CAPES); Spanish funds from Ministerio de Economía y Competitividad, Instituto de Salud Carlos III-FEDER-ERDF Grants PI16/00742 and PI19/00264 (to A.P.D.); and FAPESP Postdoctoral Fellow Grants 2017/25116-2 and 2019/26376-0 (to T.J.C.).

## DISCLOSURES

No conflicts of interest, financial or otherwise, are declared by the authors.

## AUTHOR CONTRIBUTIONS

T.J.C., F.V.G., A.P.D., and R.C.T. conceived and designed research; T.J.C., P.R.B., D.A.D., J.A.S.-N., S.C.H., T.S.-S., and F.J.-A. performed experiments; T.J.C., F.V.G., E.H.A., F.J.-A., A.P.D., and R.C.T. analyzed data; T.J.C., C.M.C.-N., E.H.A., C.G.M., A.P.D., and R.C.T. interpreted results of experiments; T.J.C. and A.P.D. prepared figures; T.J.C., F.J.-A., A.P.D., and R.C.T. drafted manuscript; T.J.C., P.R.B., D.A.D., J.A.S.-N., T.S.-S., C.M.C.-N., F.V.G., E.H.A., C.G.M., F.J.-A., A.P.D., and R.C.T. edited and revised manuscript; T.J.C., P.R.B., D.A.D., J.A.S.-N., S.C.H., T.S.-S., C.M.C.-N., F.V.G., E.H.A., C.G.M., F.J.-A., A.P.D., and R.C.T. approved final version of manuscript.

## REFERENCES


1. **El Khoudary SR**, **Aggarwal B**, **Beckie TM**, **Hodis HN**, **Johnson AE**, **Langer RD**, **Limacher MC**, **Manson JE**, **Stefanick ML**, **Allison MA**; **American Heart Association Prevention Science Committee of the Council on Epidemiology and Prevention; and Council on Cardiovascular and Stroke Nursing.** Menopause transition and cardiovascular disease risk: implications for timing of early prevention: a scientific statement from the American Heart Association. *Circulation* 142: e506–e532, 2020. doi:10.1161/CIR.0000000000000912.
2. **Niccoli T**, **Partridge L.** Ageing as a risk factor for disease. *Curr Biol* 22: R741–R752, 2012. doi:10.1016/j.cub.2012.07.024.
3. **Appelros P**, **Stegmayr B**, **Terént A.** Sex differences in stroke epidemiology: a systematic review. *Stroke* 40: 1082–1090, 2009. doi:10.1161/STROKEAHA.108.540781.
4. **Levine DA**, **Gross AL**, **Briceño EM**, **Tilton N**, **Giordani BJ**, **Sussman JB**, **Hayward RA**, **Burke JF**, **Hingtgen S**, **Elkind MSV**, **Manly JJ**, **Gottesman RF**, **Gaskin DJ**, **Sidney S**, **Sacco RL**, **Tom SE**, **Wright CB**, **Yaffe K**, **Galecki AT.** Sex differences in cognitive decline among US adults. *JAMA Netw Open* 4: e210169, 2021. doi:10.1001/jamanetworkopen.2021.0169.
5. **Ogola BO**, **Abshire CM**, **Visniauskas B**, **Kiley JX**, **Horton AC**, **Clark-Patterson GL**, **Kilanowski-Doroh I**, **Diaz Z**, **Bicego AN**, **McNally AB**, **Zimmerman MA**, **Groban L**, **Trask AJ**, **Miller KS**, **Lindsey SH.** Sex differences in vascular aging and impact of GPER deletion. *Am J Physiol Heart Circ Physiol* 323: H336–H349, 2022. doi:10.1152/ajpheart.00238.2022.
6. **Liguori I**, **Russo G**, **Curcio F**, **Bulli G**, **Aran L**, **Della-Morte D**, **Gargiulo G**, **Testa G**, **Cacciatore F**, **Bonaduce D**, **Abete P.** Oxidative stress, aging, and diseases. *Clin Interv Aging* 13: 757–772, 2018. doi:10.2147/CIA.S158513.
7. **Tang EH**, **Vanhoutte PM.** Gene expression changes of prostanoid synthases in endothelial cells and prostanoid receptors in vascular smooth muscle cells caused by aging and hypertension. *Physiol Genomics* 32: 409–418, 2008. doi:10.1152/physiolgenomics.00136.2007.
8. **Balasubramanian P**, **Hall D**, **Subramanian M.** Sympathetic nervous system as a target for aging and obesity-related cardiovascular diseases. *Geroscience* 41: 13–24, 2019. doi:10.1007/s11357-018-0048-5.
9. **Esler MD**, **Thompson JM**, **Kaye DM**, **Turner AG**, **Jennings GL**, **Cox HS**, **Lambert GW**, **Seals DR.** Effects of aging on the responsiveness of the human cardiac sympathetic nerves to stressors. *Circulation* 91: 351–358, 1995. doi:10.1161/01.cir.91.2.351.
10. **Willie CK**, **Tzeng YC**, **Fisher JA**, **Ainslie PN.** Integrative regulation of human brain blood flow. *J Physiol* 592: 841–859, 2014. doi:10.1113/jphysiol.2013.268953.
11. **Novella S**, **Dantas AP**, **Segarra G**, **Novensà L**, **Bueno C**, **Heras M**, **Hermenegildo C**, **Medina P.** Gathering of aging and estrogen withdrawal in vascular dysfunction of senescent accelerated mice. *Exp Gerontol* 45: 868–874, 2010. doi:10.1016/j.exger.2010.07.007.
12. **Novella S**, **Dantas AP**, **Segarra G**, **Novensa L**, **Heras M**, **Hermenegildo C**, **Medina P.** Aging enhances contraction to thromboxane A2 in aorta from female senescence-accelerated mice. *Age (Dordr)* 35: 117–128, 2013. doi:10.1007/s11357-011-9337-y.
13. **Onetti Y**, **Jiménez-Altayó F**, **Heras M**, **Vila E**, **Dantas AP.** Western-type diet induces senescence, modifies vascular function in non-senescence mice and triggers adaptive mechanisms in senescent ones. *Exp Gerontol* 48: 1410–1419, 2013. doi:10.1016/j.exger.2013.09.004.
14. **Miyamoto M.** Characteristics of age-related behavioral changes in senescence-accelerated mouse SAMP8 and SAMP10. *Exp Gerontol* 32: 139–148, 1997. doi:10.1016/s0531-5565(96)00061-7.
15. **Cosín-Tomás M**, **Álvarez-López MJ**, **Companys-Alemany J**, **Kaliman P**, **González-Castillo C**, **Ortuño-Sahagún D**, **Pallàs M**, **Griñán-Ferré C.** Temporal integrative analysis of mRNA and microRNAs expression profiles and epigenetic alterations in female SAMP8, a model of age-related cognitive decline. *Front Genet* 9: 596, 2018. doi:10.3389/fgene.2018.00596.
16. **Butterfield D**, **Poon H.** The senescence-accelerated prone mouse (SAMP8): a model of age-related cognitive decline with relevance to alterations of the gene expression and protein abnormalities in Alzheimer's disease. *Exp Gerontol* 40: 774–783, 2005. doi:10.1016/j.exger.2005.05.007.
17. **Costa TJ**, **Jiménez-Altayó F**, **Echem C**, **Akamine EH**, **Tostes R**, **Vila E**, **Dantas AP**, **Carvalho MHC.** Late onset of estrogen therapy impairs carotid function of senescent females in association with altered prostanoid balance and upregulation of the variant ERα36. *Cells* 8: 1217, 2019. doi:10.3390/cells8101217.
18. **Gomes FV**, **Grace AA.** Prefrontal cortex dysfunction increases susceptibility to schizophrenia-like changes induced by adolescent stress exposure. *Schizophr Bull* 43: 592–600, 2017. doi:10.1093/schbul/sbw156.
19. **Proudman RGW**, **Pupo AS**, **Baker JG.** The affinity and selectivity of α-adrenoceptor antagonists, antidepressants, and antipsychotics for the human α1A, α1B, and α1D-adrenoceptors. *Pharmacol Res Perspect* 8: e00602, 2020. doi:10.1002/prp2.602.
20. **Jiménez-Altayó F**, **Onetti Y**, **Heras M**, **Dantas AP**, **Vila E.** Western-style diet modulates contractile responses to phenylephrine differently in mesenteric arteries from senescence-accelerated prone (SAMP8) and resistant (SAMR1) mice. *Age (Dordr)* 35: 1219–1234, 2013. doi:10.1007/s11357-012-9450-6.
21. **Credeur DP**, **Holwerda SW**, **Boyle LJ**, **Vianna LC**, **Jensen AK**, **Fadel PJ.** Effect of aging on carotid baroreflex control of blood pressure and leg vascular conductance in women. *Am J Physiol Heart Circ Physiol* 306: H1417–H1425, 2014. doi:10.1152/ajpheart.00036.2014.
22. **Omar NM**, **Abbas AM**, **Abdel-Malek H**, **Suddek GM.** Effect of age on the contractile response of the rat carotid artery in the presence of sympathetic drugs and L-NAME. *Acta Physiol Hung* 100: 266–279, 2013. doi:10.1556/APhysiol.100.2013.3.3.
23. **de Oliveira AM**, **Campos-Mello C**, **Leitão MC**, **Correa FM.** Maturation and aging-related differences in responsiveness of rat aorta and carotid arteries to $\alpha_1$-adrenoceptor stimulation. *Pharmacology* 57: 305–313, 1998. doi:10.1159/000028256.
24. **Sverdlov AL**, **Ngo DT**, **Chan WP**, **Chirkov YY**, **Horowitz JD.** Aging of the nitric oxide system: are we as old as our NO? *J Am Heart Assoc* 3: e000973, 2014. doi:10.1161/JAHA.114.000973.
25. **Goubareva I**, **Gkaliagkousi E**, **Shah A**, **Queen L**, **Ritter J**, **Ferro A.** Age decreases nitric oxide synthesis and responsiveness in human platelets and increases formation of monocyte-platelet aggregates. *Cardiovasc Res* 75: 793–802, 2007. doi:10.1016/j.cardiores.2007.05.021.
26. **Barros PC**, **Costa TJ**, **Akamine EH**, **Tostes RC.** Vascular aging in rodent models: contrasting mechanisms driving the female and male vascular senescence. *Front Aging* 2: 727604, 2021. doi:10.3389/fragi.2021.727604.
27. **Felicio LS**, **Nelson JF**, **Finch CE.** Longitudinal studies of estrous cyclicity in aging C57BL/6J mice: II. Cessation of cyclicity and the duration of persistent vaginal cornification. *Biol Reprod* 31: 446–453, 1984. doi:10.1095/biolreprod31.3.446.
28. **Han J**, **Hosokawa M**, **Umezawa M**, **Yagi H**, **Matsushita T**, **Higuchi K**, **Takeda T.** Age-related changes in blood pressure in the senescence-accelerated mouse (SAM): aged SAMP1 mice manifest hypertensive vascular disease. *Lab Anim Sci* 48: 256–263, 1998.
29. **Takahashi TA**, **Johnson KM.** Menopause. *Med Clin North Am* 99: 521–534, 2015. doi:10.1016/j.mcna.2015.01.006.
30. **Majesky MW.** Developmental basis of vascular smooth muscle diversity. *Arterioscler Thromb Vasc Biol* 27: 1248–1258, 2007. doi:10.1161/ATVBAHA.107.141069.
31. **Pfaltzgraff ER**, **Shelton EL**, **Galindo CL**, **Nelms BL**, **Hooper CW**, **Poole SD**, **Labosky PA**, **Bader DM**, **Reese J.** Embryonic domains of the aorta derived from diverse origins exhibit distinct properties that converge into a common phenotype in the adult. *J Mol Cell Cardiol* 69: 88–96, 2014. doi:10.1016/j.yjmcc.2014.01.016.
32. **Frost M**, **Keable A**, **Baseley D**, **Sealy A**, **Andreea Zbarcea D**, **Gatherer M**, **Yuen HM**, **Sharp MM**, **Weller RO**, **Attems J**, **Smith C**, **Chiarot PR**, **Carare RO.** Vascular α1A adrenergic receptors as a potential therapeutic target for IPAD in Alzheimer's disease. *Pharmaceuticals (Basel)* 13: 261, 2020. doi:10.3390/ph13090261.
33. **Kara B**, **Gordon MN**, **Gifani M**, **Dorrance AM**, **Counts SE.** Vascular and nonvascular mechanisms of cognitive impairment and dementia. *Clin Geriatr Med* 39: 109–122, 2023. doi:10.1016/j.cger.2022.07.006.
34. **Fouda AY**, **Fagan SC**, **Ergul A.** Brain vasculature and cognition. *Arterioscler Thromb Vasc Biol* 39: 593–602, 2019. doi:10.1161/ATVBAHA.118.311906.

35. **Heller S**, **Hines G.** Carotid stenosis and impaired cognition: the effect of intervention. *Cardiol Rev* 25: 211–214, 2017. doi:10.1097/CRD.0000000000000139.
36. **Dutra AP.** Cognitive function and carotid stenosis: review of the literature. *Dement Neuropsychol* 6: 127–130, 2012. doi:10.1590/S1980-57642012DN06030003.
37. **Wang A**, **Liu X**, **Chen G**, **Hao H**, **Wang Y**, **Wang Y.** Association between carotid plaque and cognitive impairment in Chinese stroke population: the SOS-Stroke Study. *Sci Rep* 7: 3066, 2017. doi:10.1038/s41598-017-02435-3.
38. **Zhong W**, **Cruickshanks KJ**, **Schubert CR**, **Acher CW**, **Carlsson CM**, **Klein BE**, **Klein R**, **Chappell RJ.** Carotid atherosclerosis and 10-year changes in cognitive function. *Atherosclerosis* 224: 506–510, 2012. doi:10.1016/j.atherosclerosis.2012.07.024.
39. **Pettigrew LC**, **Thomas N**, **Howard VJ**, **Veltkamp R**, **Toole JF.** Low mini-mental status predicts mortality in asymptomatic carotid arterial stenosis. Asymptomatic carotid atherosclerosis study investigators. *Neurology* 55: 30–34, 2000. doi:10.1212/wnl.55.1.30.
40. **Mitchell GF**, **van Buchem MA**, **Sigurdsson S**, **Gotal JD**, **Jonsdottir MK**, **Kjartansson Ó**, **Garcia M**, **Aspelund T**, **Harris TB**, **Gudnason V**, **Launer LJ.** Arterial stiffness, pressure and flow pulsatility and brain structure and function: the Age, Gene/Environment Susceptibility–Reykjavik study. *Brain* 134: 3398–3407, 2011. doi:10.1093/brain/awr253.